Seafloor Mapping from High-Density Satellite Altimetry

NICOLAS BAUDRY[1] and STEPHANE CALMANT[2]

[1] *Seafloor Imaging Inc., BP 8039, 98807 Nouméa Sud, New Caledonia*
[2] *Institut Français de Recherche Scientifique pour le Développement en Coopération (ORSTOM), BP A5, 98848 Nouméa Cedex, New Caledonia*

(Received 4 May 1995; accepted 8 September 1995)

Key words: Satellite altimetry, marine gravity, bathymetric maps.

Abstract. In this paper, we publish the results of a bathymetry survey based on the processing of satellite altimetry data. Data gathered from GEOSAT (Geodetic Mission), SEASAT, ERS-1 and TOPEX/POSEIDON satellites were processed to recover the seafloor topography over new seamounts in a test area located in the south central Pacific. We show that by processing high-density satellite altimetry data, alone or in combination with shiptrack bathymetric data, it is possible to produce full coverage bathymetric maps.

Introduction

One of the most significant developments to have occurred in the field of marine geophysics over the last two decades is the use of radar altimeters aboard oceanographic satellites (see a review of applications in Sandwell, 1991). The radar altimeters measure the distance from the satellite to the subsatellite point (nadir) on the ocean surface with an accuracy of a few centimeters. The path of the orbit, which can be measured independently, is combined with satellite altimeter data to produce accurate measurements of the shape of the ocean's surface along the satellite track. The radar footprint on the sea surface is about 1 km but measurements are averaged every 7 km along the track.

The ocean flows under the influence of gravity: in the absence of disturbing forces, its surface conforms to the shape of an equipotential surface of the Earth's gravity field. This surface is called the geoid. It follows that satellite altimeter data give an indirect measurement of the variations of the Earth's gravity field. The process is impeded by oceanic features such as rings, eddies and currents. Long-term averages of sea surface heights reduce the impact of any noise introduced by these oceanographic features and result in a mean sea surface that closely approximates the marine geoid. These averages are arrived at by using data from Exact Repeat Missions (GEOSAT between 1987 and 1989, TOPEX/POSEIDON and ERS-1 between 1991 and 1994). On the other hand, Geodetic Missions (GEOS-3, SEASAT, GEOSAT beween 1986 and 1987 and ERS-1 in 1994) produce data with very good spatial coverage. Nowadays, spatial resolution is better than 15 km and the accuracy (altimetric noise) has been improved from 30 cm for GEOS-3 to better than 5 cm for TOPEX/POSEIDON and ERS-1. The GEOS-3 (1975) and SEASAT (1978) satellites have demonstrated the potential of satellite altimetry for the recovery of the Earth gravity equipotential surface over the oceans. The GEOSAT, ERS-1 and TOPEX/POSEIDON missions have nearly achieved the full potential of this method.

One of the major achievements in the use of satellite altimetry in marine geophysics has been the mapping and characterization of seamounts. The seafloor topography is the shallowest density interface under the sea surface, thus generating pronounced short wavelength undulations in the geoid with significant amplitudes (0.3 to 2 m height). Various methods to process the altimeter data in order to detect and, whenever possible, map the uncharted seamounts have been developed (see for instance Dixon and Parke, 1983; Sandwell, 1984; Baudry *et al.*, 1987; Vogt and Jung, 1991; Baudry and Calmant, 1991; Jung and Vogt, 1992; Smith and Sandwell, 1994; Calmant, 1994). A detailed review and discussion on these methods can be found in Calmant and Baudry (this issue). In Calmant (1994), the theoritical ability to use altimetric data in seamount topography recovery is reviewed. Satellite data acquired since the SEASAT mission are shown to be sufficiently accurate to recover the topography of seamounts with less that 100 m rms errors, provided that the coverage is dense enough in relation to the roughness of the bathymetry.

In this paper, we publish the results of a satellite survey of the seafloor performed in the southern Pacific Ocean (Figure 1). The data used are the high density GEOSAT Geodetic Mission data, combined with the data from the SEASAT, TOPEX/POSEIDON and ERS-1 satellites.

Marine Geophysical Researches **18:** 135–146, 1996.

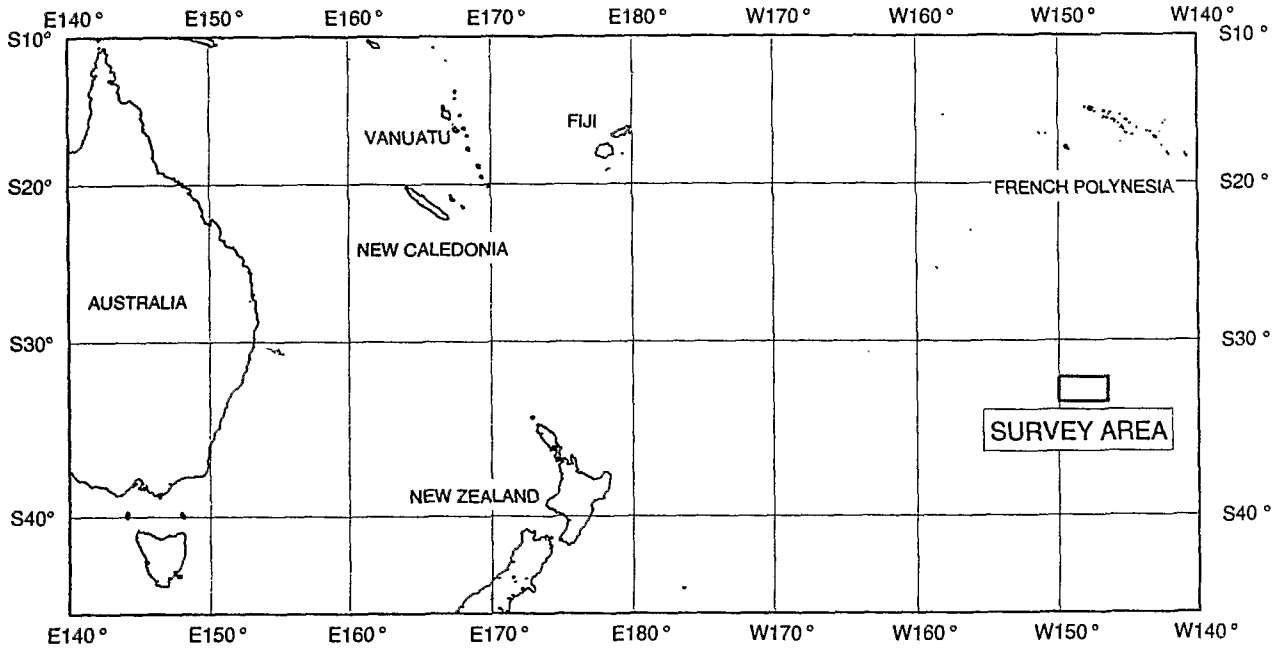

Fig. 1. Location of the study area.

The Survey Area

The survey area (Figures 1 and 2) covers about 50,000 square kilometers in the south central Pacific. The GEBCO map and the ETOPO5 global bathymetric file show this area to have a flat abyssal seafloor without any seamount. Figure 2 shows the bathymetric information reported on the navigational chart edited by the French Navy (SHOM map number 7166, edition 1988, updated 1990). According to sailing instructions (Pacific Islands Pilot, 1982), the Jupiter Reef is a fringing reef which was detected in 1963. The existence of this reef is very doubtful (A. Thellier, personal communication), as is the existence of many reported seamounts and reefs in the southern part of the Pacific Ocean. As a matter of fact, the mapping of these seamounts is based on old and sparse bathymetry soundings performed aboard oceanographic or commercial vessels before the use of satellite positioning systems. Such features are reported on the navigational charts because they represent a potential hazard to navigation. However, it is highly probable that most seamounts within this area remain undetected, because ship board bathymetry measurements are extremely sparse. The only recent oceanographic ship cruise in the study area has been undertaken by the National Ocean Service onboard R/V Capt. F.J. Jones in 1993. Seabeam data have been acquired along a north-south ship track which is shown in Figure 2 by the bold line. Accurate positioning of the ship was achieved by a GPS navigation system. The bathymetric data from this cruise used in the present study is the one minute extraction from the central beam as provided by the NOAA-National Geophysical Data Center.

Figure 3 shows the coverage of all available satellite altimetry over the study area, which comprises data from the SEASAT, GEOSAT, TOPEX/POSEIDON and ERS-1 satellites. GEOS-3 data were not used because of too high a noise level. GEOSAT data have been obtained from the Geodetic Mission. One cycle of TOPEX/POSEIDON and 7 cycles of ERS-1 (Exact Repeat Mission) have been used. The purpose of this study is to process this set of high density satellite altimeter data in order to verify the existence of Jupiter Reef, and to detect and map possible seamounts east of Jupiter Reef, the existence of which is suggested by the soundings mentioned on the navigational chart.

Data Processing

The algorithms used in this study are improved versions of the algorithms published by Baudry and

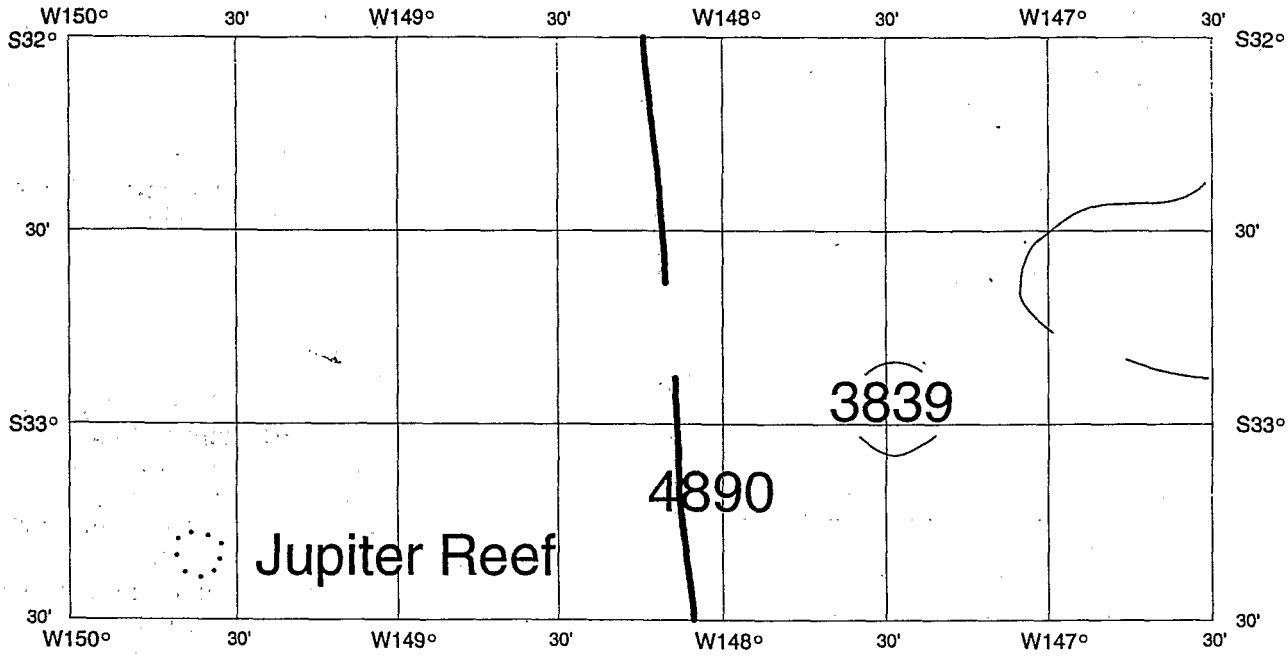

Fig. 2. Study area. Sounding information obtained from SHOM navigational chart. The bold north-south line shows the Seabeam data acquisition along the track of R/V Capt. F. J. Jones.

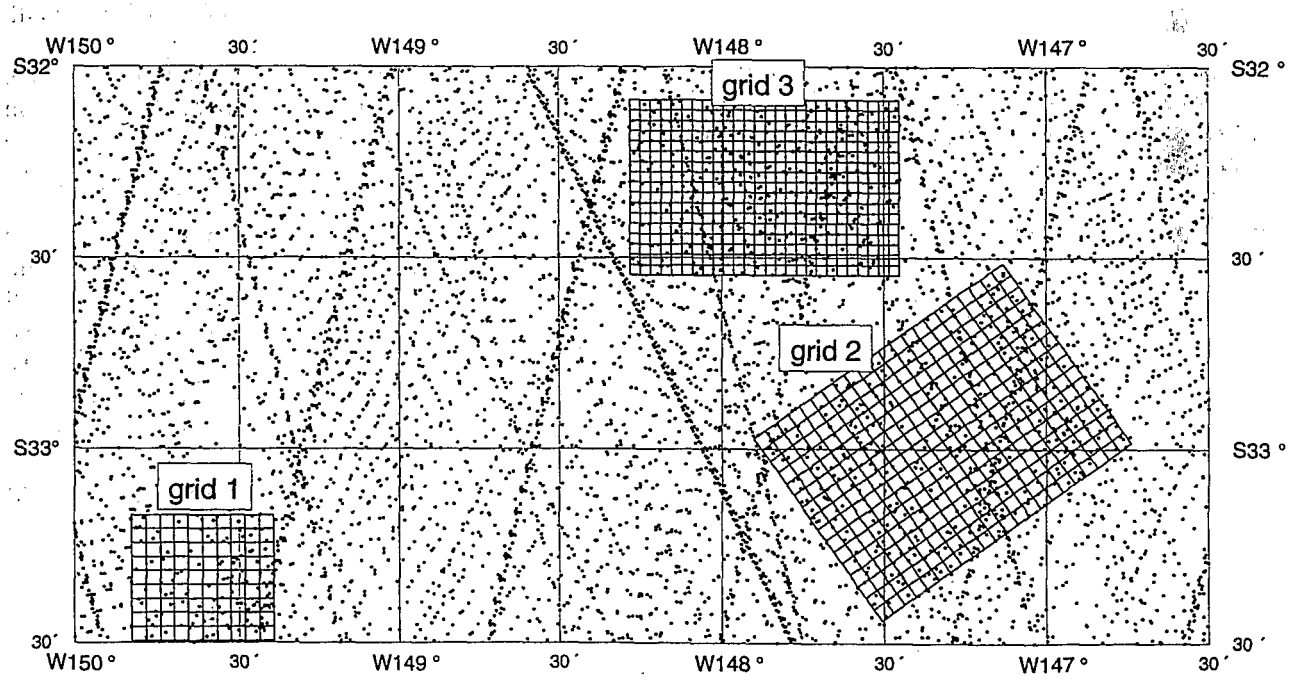

Fig. 3. Satellite altimetry data processed in this study. Data from GEOSAT (Geodetic Mission), SEASAT, TOPEX/POSEIDON, and ERS-1 (Exact Repeat Mission). The three grids have been defined to compute local geoid anomaly andassociated bathymetry.

Calmant (1991). All processing algorithms have been assembled in a unix-based interactive software which allows the handling and processing of both marine and satellite data.

Computing geoid height anomalies from altimetry measurements

To obtain a regular grid of the geoid height anomaly, the along-track sea surface height measurements $n(\mathbf{s})$ are interpolated using a collocation scheme (Moritz, 1978) to generate geoid values over a regular grid $n(\mathbf{r})$ suitable for further processing in the Fourier space:

$$n(\mathbf{r}) = C(\mathbf{r}, \mathbf{s})[C(\mathbf{s}, \mathbf{s}) + E(\mathbf{s}, \mathbf{s})]^{-1} n(\mathbf{s}). \quad (1)$$

Collocation is the implementation of an interpolator in the space domain constructed by means of the spectral content of the physical field to be interpolated. This spectral content is accounted in the form of the auto-covariance $C(x)$ of the geoid, where x is the lag between either grid points or measurements. Baudry and Calmant (1991) have shown that for seamounts studies, this auto-covariance function could be satisfactorily modelled as follows:

$$C(x) = \frac{\sigma_0^2}{(1 + x/L_c)}. \quad (2)$$

In Equation (2), σ_0^2 is the signal variance and L_c the half-correlation length. Typical half-correlation lengths vary between 0.2 and 0.4 degrees, depending on the width of the geoid anomalies associated with the seafloor features to be mapped. In Equation (1), the matrix $E(\mathbf{s}, \mathbf{s})$ stands for the covariance of the data errors.

Errors are processed in two stages, according to their main wavelength.

1. At the scale the present study has been performed, the radial orbit errors and the meteo-oceanographic effects can be considered to bias each satellite track independently. These biases are removed using a classical least square scheme with a Lagrange constraint of zero average. Additional processing to remove the long-wavelength (>200 km) sea-surface variations unrelated to seafloor topography includes the removal of a potential field model (Reigber *et al.*, 1985), and the removal of a mean plane from the data (l_1 norm). Residual sea-surface heights resulting from such processing are indicated by color dots in Figures 6 and 8.
2. The instrument noise can be considered a white noise and henceforth be modelled by a Dirac pulse and integrated into the collocation-interpolation procedure by $E(\mathbf{s}, \mathbf{s})$. Amplitudes of this noise for the different instruments are given in Table I.

So processed, the major errors which pollute the data are flushed out. The results of computing the geoid height variations at the nodes of a regular grid using such a collocation algorithm are shown in Figures 5, 6 and 8 by bold contour lines.

Computing seafloor topography from geoid height anomalies

The algorithm used is based on the theoretical works of Parker (1972), Oldenburg (1974) and Banks *et al.* (1977). Basically, seafloor topography is physically equivalent to an interface between two layers of different density: the sea-water and the upper crustal layer. Deeper density constrasts within the Earth, the layer 2—layer 3 interface and the Moho interface (the interface between layer 3 and the mantle), have also to be taken into account. Indeed, in the case of volcanic constructions like the seamounts in the survey area, these two interfaces are deflected downward in response to loading. The physical parameter which determines the deformation of these interfaces is the flexural rigidity of the lithosphere D, the former being determined by the age of the Earth crust at the time of loading (Watts 1978; Watts and Ribe, 1984; Calmant *et al.*, 1990).

A first approximation of the seafloor topography $b_0(r)$ is computed in the Fourier space (Parker, 1972; Watts and Ribe, 1984) by

$$B_0(\mathbf{k}) = N(\mathbf{k}) Z(\mathbf{k})^{-1}, \quad (3)$$

where $\mathbf{k}$ is the $2D$ wave number. In this equation, $B_0(\mathbf{k})$ and $N(\mathbf{k})$ are the Fourier transforms of the computed bathymetry $b_0(\mathbf{r})$ and the observed geoid anomaly $n(\mathbf{r})$, and $Z(\mathbf{k})$ is a transfer function which integrates local geological and geophysical parameters. $Z(\mathbf{k})$ is given by (see Table I for meaning and values of constants):

$$Z(\mathbf{k}) = \frac{2\pi G}{g} |\mathbf{k}|^{-1} \{E_1(\mathbf{k}) + E_2(\mathbf{k}) \Phi(\mathbf{k})\}, \quad (4)$$

where

$$E_1(\mathbf{k}) = (\rho - \rho_0) e^{-|\mathbf{k}| z_0},$$

$$E_2(\mathbf{k}) = (\rho_2 - \rho) e^{-|\mathbf{k}| z_0} + (\rho_3 - \rho_2) e^{-|\mathbf{k}|(z_0 + t_2)} + (\rho_m - \rho_3) e^{-|\mathbf{k}|(z_0 + t_{moho})},$$

z_0 is the mean seafloor depth, the initial value of which is estimated from neighbouring shipboard bathymetry

TABLE I
Values of the constants

Name	Symbol	Value
Geoid half-correlation length	L_c	0.3°
White noise amplitude of sea-surface height measurements:		
SEASAT		10 cm
GEOSAT		8 cm
TOPEX/POSEIDON		5 cm
ERS−1		5 cm
Sea water density	ρ_0	1.02 g cm^{-3}
Load density	ρ	2.6 g cm^{-3}
Crustal layer 2 density	ρ_2	2.6 g cm^{-3}
Crustal layer 3 density	ρ_3	2.9 g cm^{-3}
Mantle density	ρ_m	3.2 g cm^{-3}
Standart depth of layer 2−layer 3 interface	t_2	2.5 km
Standart depth of moho interface	t_m	7.5 km
Gravitational constant	G	6.673×10^{-11} m^3 kg^{-1} s^{-2}
Mean gravity acceleration	g	9.81 m s^{-2}

tracks, when available, or from extrapolated values of such tracks.

$\Phi(k)$ contains the information on the shape of the deformed interfaces within the oceanic lithosphere. It is given by

$$\Phi(\mathbf{k}) = \frac{-g(\rho - \rho_0)}{D|\mathbf{k}|^4 + g(\rho_m - \rho)}. \quad (5)$$

Refined values $B_i(\mathbf{k})$ are obtained from the first approximation of the seafloor topography $B_0(\mathbf{k})$ by adding a bathymetric correction to the computed bathymetry $B_{i-1}(\mathbf{k})$. This bathymetric correction is computed using the residual values between the observed geoid anomaly $N(\mathbf{k})$ and the synthetic geoid anomaly $Q(B_{i-1}(\mathbf{k}))$ generated by the computed bathymetry $B_{i-1}(\mathbf{k})$ as

$$B_i(\mathbf{k}) = B_{i-1}(\mathbf{k}) + (N(\mathbf{k}) - Q(B_{i-1}(\mathbf{k})))Z(\mathbf{k})^{-1}. \quad (6)$$

A detailed expression of $Q(B_{i-1}(\mathbf{k}))$ is found in Baudry and Calmant (1991). It is of paramount importance to avoid the occurence and development of unrealistic short-wavelength topography undulations during the iterative computing. To prevent such numerical problems, the bathymetric correction is low-pass filtered with a Butterworth filter the cutoff wavelength of which is modified at each iteration from large values down to the Nyquist wavelength. At each iteration, the computed bathymetry is adjusted according to bathymetry at some constraint points. These constraint points are obtained from shipboard bathymetric data, when available, or from assumed bathymetry. Adjustment is made by translating the computed bathymetry vertically in order to minimize (l_1 norm) the discrepancy between bathymetry at constraint points and computed bathymetry. Constraint points are also provided for the crustal structure. At these points, the crustal interfaces are vertically translated at each iteration, in order to fit the thickness of the layers provided as parameters.

At each iteration, graphic tools allow to check the evolution of some critical functions such as:

1. The shape and depth of bathymetry and crustal interfaces.
2. The adjustment of bathymetry and crustal interfaces at constraint points.
3. The spectral content of the bathymetry and that of the residuals.
4. The adjustment between the geoid anomaly produced by computed bathymetry and the geoid anomaly from satellite data.

Usually, 20 to 30 iterations are enough to obtain a satisfactory result, i.e. a seafloor topography which generates a geoid anomaly very close to the observed one (obtained from satellite altimetry). The final bathymetry is obtained by inverse Fourier transform of the last $B_i(\mathbf{k})$ computed.

In this study, we used a standard value of 10^{22} Nm for D and 2600 kg/m^3 for ρ. Values for mean density and thickness of the different crustal layers are provided by regional geological models of the Earth crustal structure. It has been shown (Baudry and Calmant, 1991) that for small or middle sized seamounts such as intraplate volcanoes of the South Pacific, the uncertainty relating to the exact value of D generates relatively small errors on the computed bathymetry $b(\mathbf{r})$ evaluated to remain within 5% of the bathymetry amplitude. Yet, we develop an expression from which standard deviations related to uncertainties upon D and ρ can be analytically evaluated over the computation area. The standard deviation at each grid node is given by the square root of the diagonal elements of the covariance matrix of the errors upon the computed bathymetry. This covariance matrix can be obtained as the inverse Fourier transform of the spectral density $\delta P(\mathbf{k}\mathbf{k}')$ of the bathymetry variations due to variations in the transfert function, $\delta Z(\mathbf{k})^{-1}$. Using the approximation given in Equation (2), $\delta P(\mathbf{k}\mathbf{k}')$ is computed as:

$$\delta P(\mathbf{k}, \mathbf{k}') = |(N(\mathbf{k}, \mathbf{k}')\delta Z(\mathbf{k}, \mathbf{k}')^{-1})|^2. \quad (7)$$

The diagonal elements of the covariance matrix correspond to the inverse Fourier transform of

$\delta P(\mathbf{k}, \mathbf{k}')$ for $\mathbf{k}=\mathbf{k}'$. The variations in $Z(\mathbf{k})^{-1}$ due to uncertainties upon D and ρ, are computed from the partial derivatives $\partial Z(\mathbf{k})^{-1}/\partial D$ and $\partial Z(\mathbf{k})^{-1}/\partial \rho$, successively given by

$$\frac{\partial Z(\mathbf{k})^{-1}}{\partial D} = Z(\mathbf{k})^{-2} \frac{1}{D} \frac{2\pi G}{g} |\mathbf{k}|^{-1} \{E_2(\mathbf{k}) \Phi(\mathbf{k}) \Psi_D(\mathbf{k})\} \tag{8}$$

$$\frac{\partial Z(\mathbf{k})^{-1}}{\partial \rho} = Z(\mathbf{k})^{-2} \frac{1}{(\rho - \rho_0)} \frac{2\pi G}{g} |\mathbf{k}|^{-1} \times \{E_1(\mathbf{k})(1-\Phi(\mathbf{k})) + E_2(\mathbf{k}) \Phi(\mathbf{k}) \Psi_\rho(\mathbf{k})\} \tag{9}$$

with

$$\Psi_D(\mathbf{k}) = \frac{-D|\mathbf{k}|^4}{g(\rho_m - \rho)}$$

and

$$\Psi_\rho(\mathbf{k}) = \frac{D|\mathbf{k}|^4 + g(\rho_m - \rho_0)}{D|\mathbf{k}|^4 + g(\rho_m - \rho)}.$$

From (7), (8) and (9), the bathymetry uncertainties $\sigma_b(\mathbf{r})$ are thus:

$$\sigma_b(\mathbf{r}) = |N(\mathbf{k}) Z(\mathbf{k})^{-2}|^2 \times \left\{ \left[\sigma_\rho \frac{\partial Z(\mathbf{k})^{-1}}{\partial \rho} \right]^2 + \left[\frac{3\sigma_{T_e}}{T_e} \frac{\partial Z(\mathbf{k})^{-1}}{\partial D} \right]^{-2} \right\}. \tag{10}$$

In Equation (10), the uncertainty σ_{T_e} upon the elastic thickness T_e equivalent to the plate stiffness is used instead of the uncertainty upon the stiffness itself, using

$$\frac{\delta D}{D} = 3 \frac{\delta T_e}{T_e}.$$

Results

Preliminary imagery of the seafloor topography

A preliminary imagery of the seafloor topography is obtained by mapping the sea-surface undulations in the 0-200 km wavelength band. All satellite tracks available over the study area (Figure 3) have been high-pass filtered using a Butterworth, 3rd order, high-pass filter. The resulting geoid variations are shown in Figure 4 and are color coded to enhance the positive geoid signature of seafloor features such as seamounts and chains. This image identifies all main seafloor positive variations (above mean abyssal depth) throughout the area. The use of high-density satellite altimetry allows a 100 percent coverage of the area for the detection of seamounts of significant height.

Checking bathymetric maps and navigational charts

According to sailing instructions and navigational charts, the location of Jupiter Reef is 33°22′ S, 149°38′ W. No significant geoid height anomaly appears over the expected location of Jupiter Reef on the filtered geoid map shown in Figure 4. A more in-depth examination of the satellite altimeter data at the expected location of Jupiter Reef is given in Figure 5. On this figure, dots represent satellite data measurements. Satellite data within the green polygon have been processed as described above (first step of data processing), except that the mean plane has not been removed from the data in order to show that no strong gradient exists in the geoid in the vicinity of Jupiter Reef. Color dots show the residual sea surface height values. These residual values have then been used to compute the geoid anomaly over a grid (4 km grid step) centered on the reported location of Jupiter Reef, using the collocation algorithm described above. The resulting geoid anomaly is shown by black contour lines (isoline spacing = 5 cm). Grid node locations are shown in Figure 3 (grid 1). If a fringing reef or a large seamount reaching the surface were present at the expected location of Jupiter Reef, the associated geoid anomaly would be a broad, high amplitude (about 1 meter) anomaly easily detectable from satellite altimetry. It is plain, from the processed satellite data, that there is no such large bathymetric feature at this location.

Computing seafloor bathymetry with no constraints from direct shipboard sounding data

The filtered sea surface height undulations map (Figure 4) reveals a cluster of two seamounts in the eastern part of the study area. Figure 6 shows the processed satellite data over this feature. As in Figure 5, dots represent the available satellite altimeter data, color dots the processed data, and the dark isoline function, the geoid anomaly (5 cm line spacing) computed at each node of a grid of 4 km grid step using the collocation algorithm (grid node locations are shown in Figure 3, grid 2). The computed geoid anomaly clearly

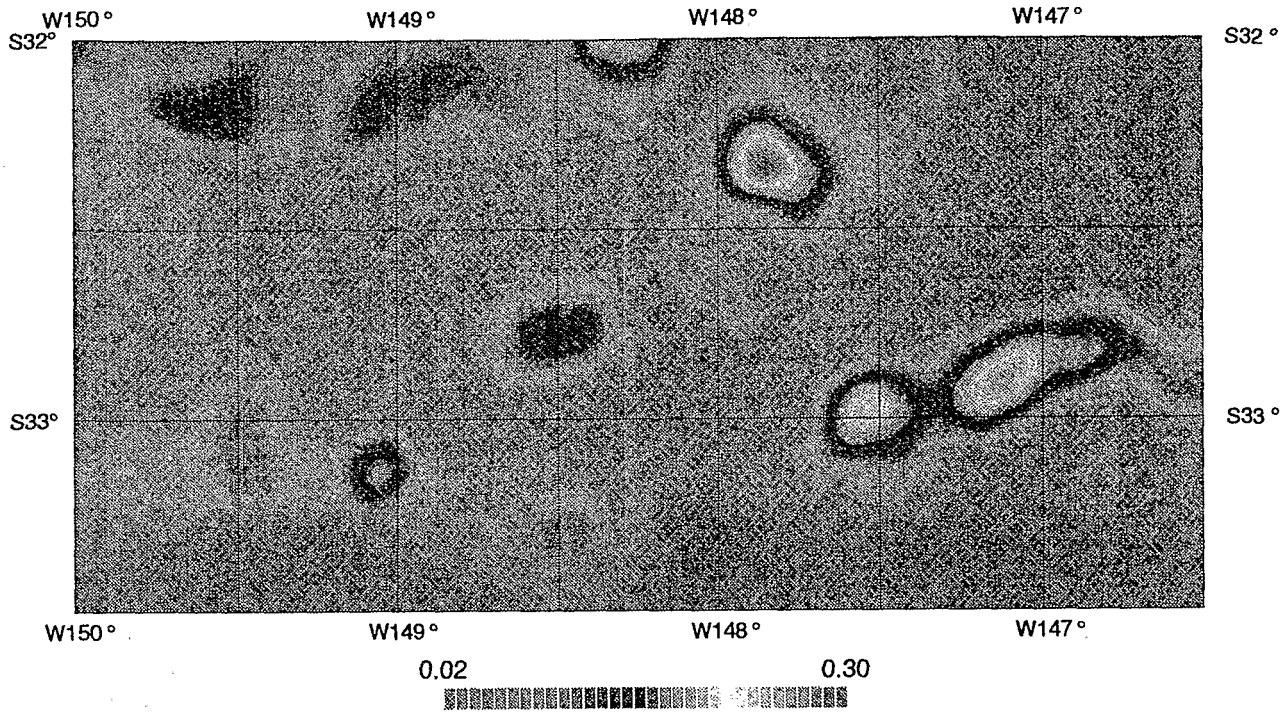

Fig. 4. Residual sea surface height undulations obtained by high-pass filtering of data along satellite tracks. Positive undulations are the signature of seafloor features such as seamounts and ridges.

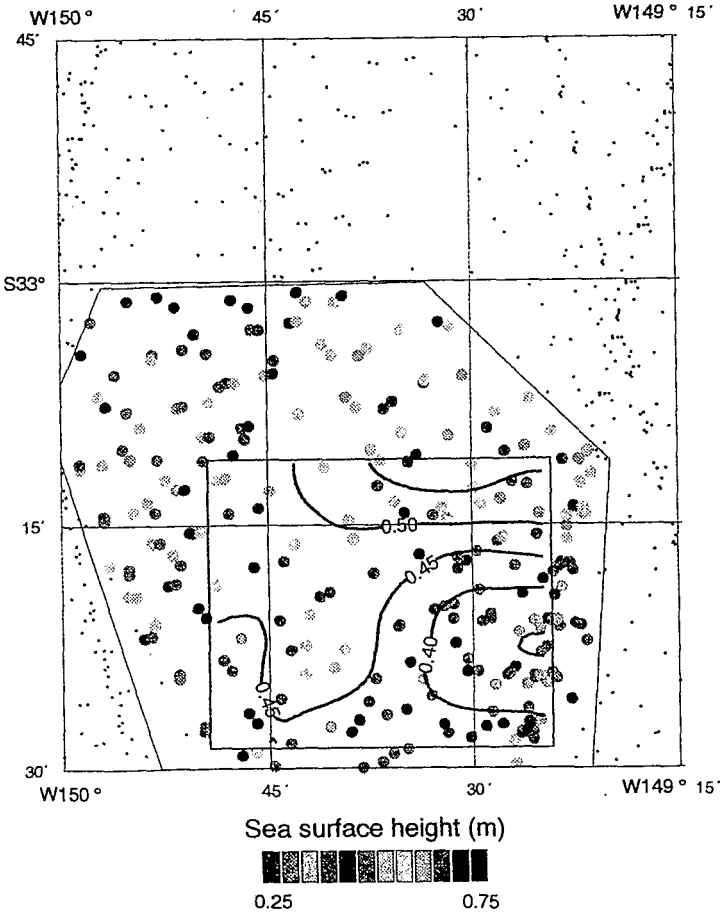

Fig. 5. Dots show the location of available satellite data. Color dots show the result of the preliminary processing of satellite altimeter data. Bold contour lines show the geoid anomaly computed at the nodes of a regular grid (4 km grid step) centered on the expected location of Jupiter Reef.

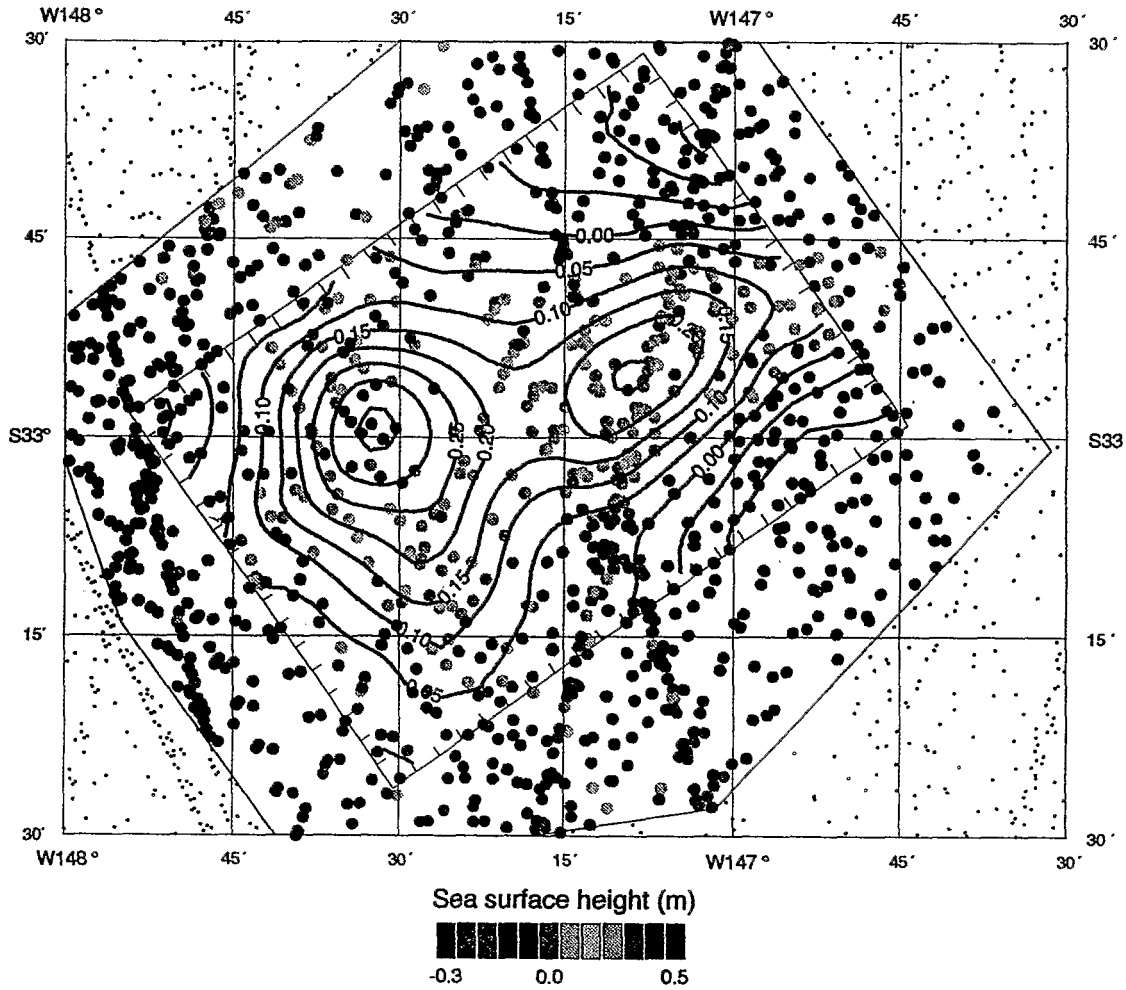
W148°
45′
30′
15′
W147°
45′
30′
S33°
0.00
0.05
0.10
0.15
0.20
Sea surface height (m)
-0.3
0.0
0.5

Fig. 6

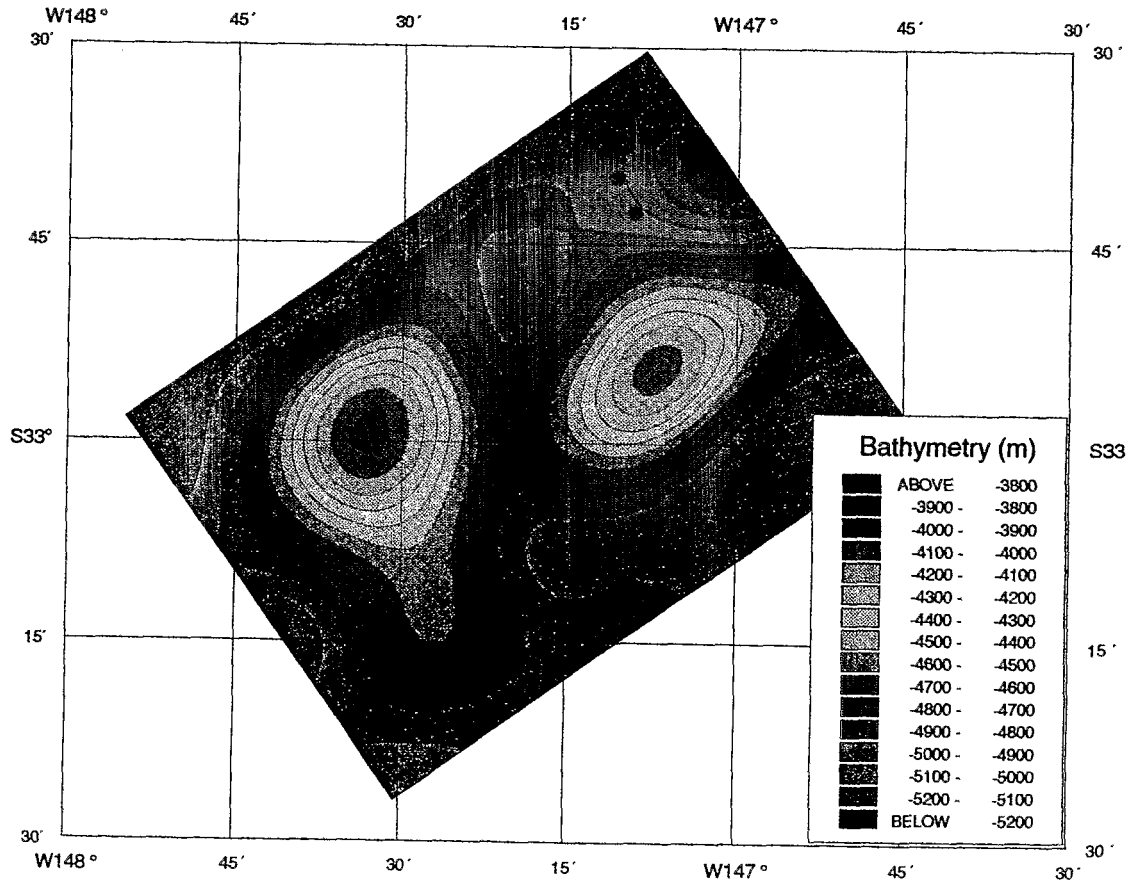
W148°
45′
30′
15′
W147°
45′
30′
S33°
Bathymetry (m)
ABOVE -3800
-3900 - -3800
-4000 - -3900
-4100 - -4000
-4200 - -4100
-4300 - -4200
-4400 - -4300
-4500 - -4400
-4600 - -4500
-4700 - -4600
-4800 - -4700
-4900 - -4800
-5000 - -4900
-5100 - -5000
-5200 - -5100
BELOW -5200

Fig. 7

shows a two summit anomaly of about 40 cm amplitude. From this geoid anomaly, the associated seafloor undulation has been computed using the iterative algorithm described above. The results are shown in Figure 7. No direct shipboard bathymetry soundings are available in marine geophysical data banks over the computing grid. Therefore, we have used as bathymetry constraint points some arbitrary points shown by the five red dots. At the location of each red dot, the seafloor depth has been assumed to be –5000 m, which is the mean abyssal depth in the area according to bathymetric maps. The same five points have been used to constraint the crustal structure. At these points, the crustal structure has been assumed to be standard, that is unperturbated by volcanic loading. The bathymetry shown in Figure 7 has been obtained after 30 iterations. The maximum discrepancy between the geoid anomaly created by the computed bathymetry and the grid of geoid anomaly is 6 cm, while the standard deviation of these discreancies over the grid is 1.5 cm. After the last iteration, the discrepancy between the computed bathymetry and the assumed bathymetry at the red dots is 82 m (standard deviation of the 5 values). This low value shows that the choice of the bathymetry constraint points is coherent with the shape of the geoid anomaly. The computed bathymetry is a cluster of two seamounts with summit depths of –3897 m (western summit) and –4020 m (eastern summit). The location and depth of the western summit is coherent with the –3839 m sounding reported on the navigational charts.

Computing seafloor bathymetry with constraints from shipboard sounding data

A second bathymetry modelling has been performed over a large geoid anomaly in the northern part of the study area. No sounding is reported at this location on the navigational charts. The processed altimeter data are shown by color dots in Figure 8. Geoid anomaly has been computed using the collocation algorithm at the nodes of a grid (3 km grid step) centered on the peak of the anomaly (grid node locations are shown in Figure 3, grid 3). The resulting geoid is shown by black isolines (5 cm isoline spacing). The anomaly amplitude is about 50 cm. Figure 9 shows the result of the bathymetry computed from this geoid anomaly. In this case, bathymetric constraint points have been provided by the one minute extraction from the Seabeam central beam shown by the color N–S track. The 105 bathymetry data located inside the computation area have been used to constraint the bathymetric solution by vertical translation at each computing iteration. The constraint points for the crustal model are shown by the white dots. The shape of the computed bathymetry is coherent with the shipboard bathymetric data along the Seabeam track. The standard deviation of the discrepancies between the measured and the computed depths is 192 m (105 measurements). The computed depth of the seamount summit is –3200 m.

Production of bathymetric maps

The bathymetry obtained on the two grids and the data from the Seabeam central beam has been re-interpolated over a grid (3 km grid spacing) using a bilinear interpolating algorithm, contoured, and result is shown in Figure 10. From a practical point of view, the technique we have developed to compute seafloor topography with bathymetry constraint points allows the production of bathymetric maps of specific areas which are consistent with bathymetry data along ship tracks. Computed bathymetry on grids and shipboard data can be merged to produce regional bathymetric maps which integrate all bathymetric information available (from ship cruises and from satellite altimetry). This technique has been successfully applied to produce new maps of the seafloor topography within the Exclusive Economic Zones of Tuvalu, Papua New-Guinea, Niue, Madagascar, La Réunion Island, and some other island countries of the Indian and Pacific oceans.

Computing bathymetric standard deviations

Since we are dealing with the detection and mapping of previously unknown bathymetric features, the tectonic setting of these structures is only guessed. The standard deviations in bathymetry due to an uncertainty $\sigma_p =$ 150 kg/m3 on the density of the load and an uncertainty $\sigma_{T_e} = 7$ km on the elastic plate thickness are shown in Figure 11. Note that in order to present a conservative evaluation of the deviations, both values of uncertainty overestimate the actual uncertainty upon the physical parameters. However, these deviations remain below 170 m. In fact, because of the limited size of the bathymetric features present in this

↖ Fig. 6. Satellite altimetry processing over a cluster of two seamounts in the eastern part of the study area. Dots show the location of satellite altimeter data, color dots the processed data, and bold contour lines the computed geoid anomaly at the nodes of a grid (4 km grid step).

← Fig. 7. Bathymetry computed from the geoid anomaly in Figure 6. Red dots show the location of constraint points for seafloor depth and crustal interfaces depths.

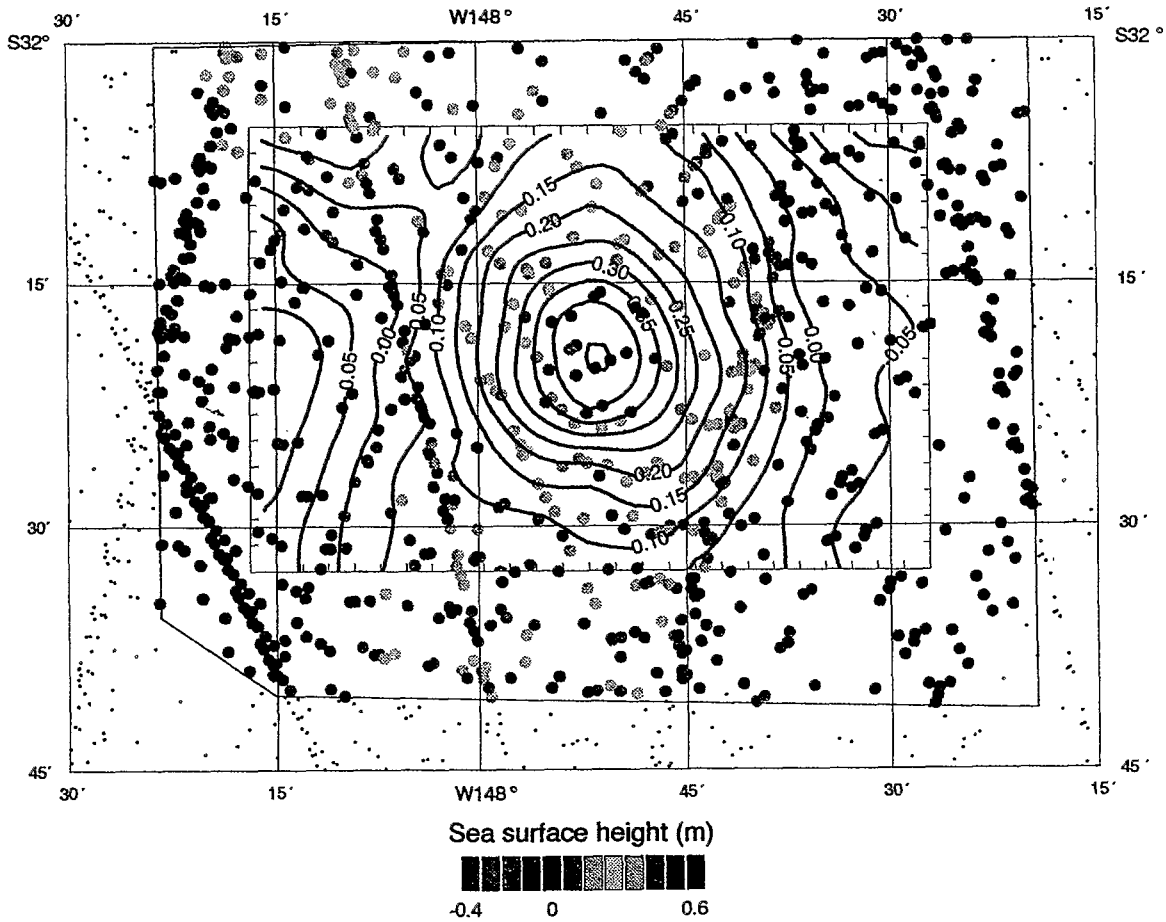

Fig. 8. Same as Figure 6 over a seamount in the northern part of the study area.

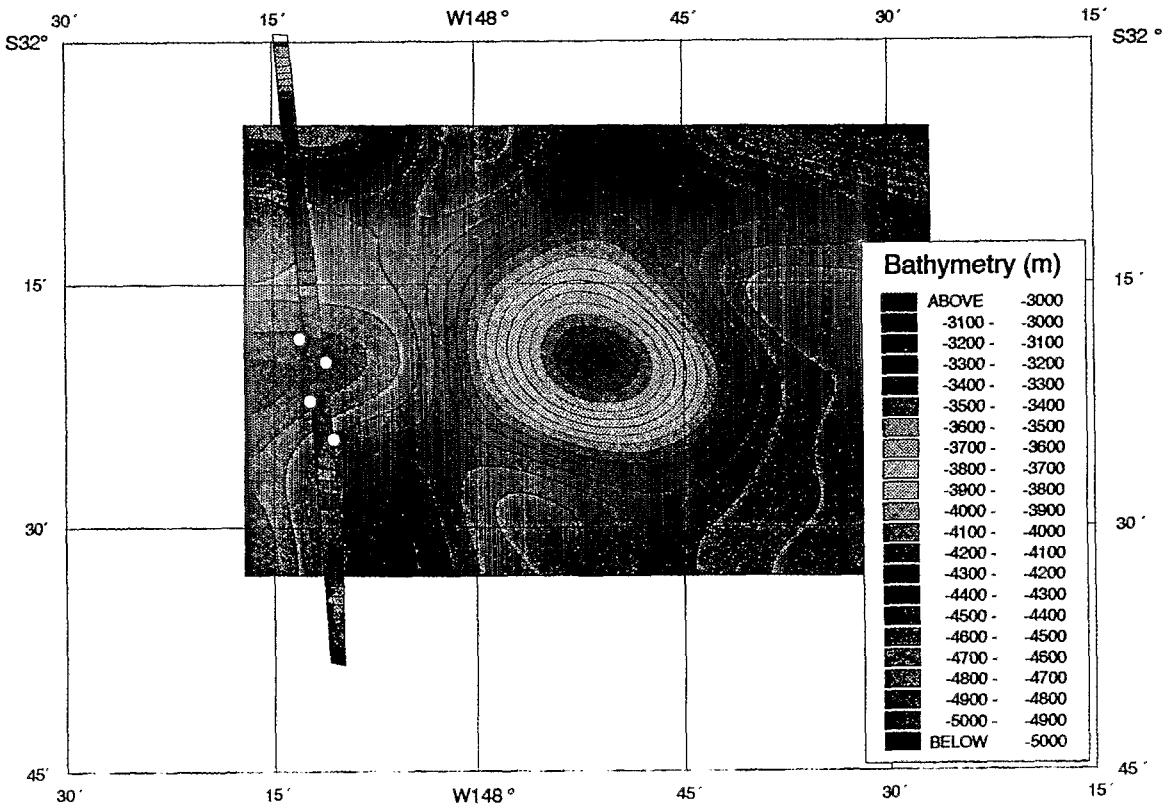

Fig. 9. Bathymetry computed from the geoid anomaly in Figure 8. Constraints points for the seafloor depth are provided by the Seabeam central beam data from the R/V JONES cruise (N-S track). White dots show the location of constraint points for the crustal interface depths.

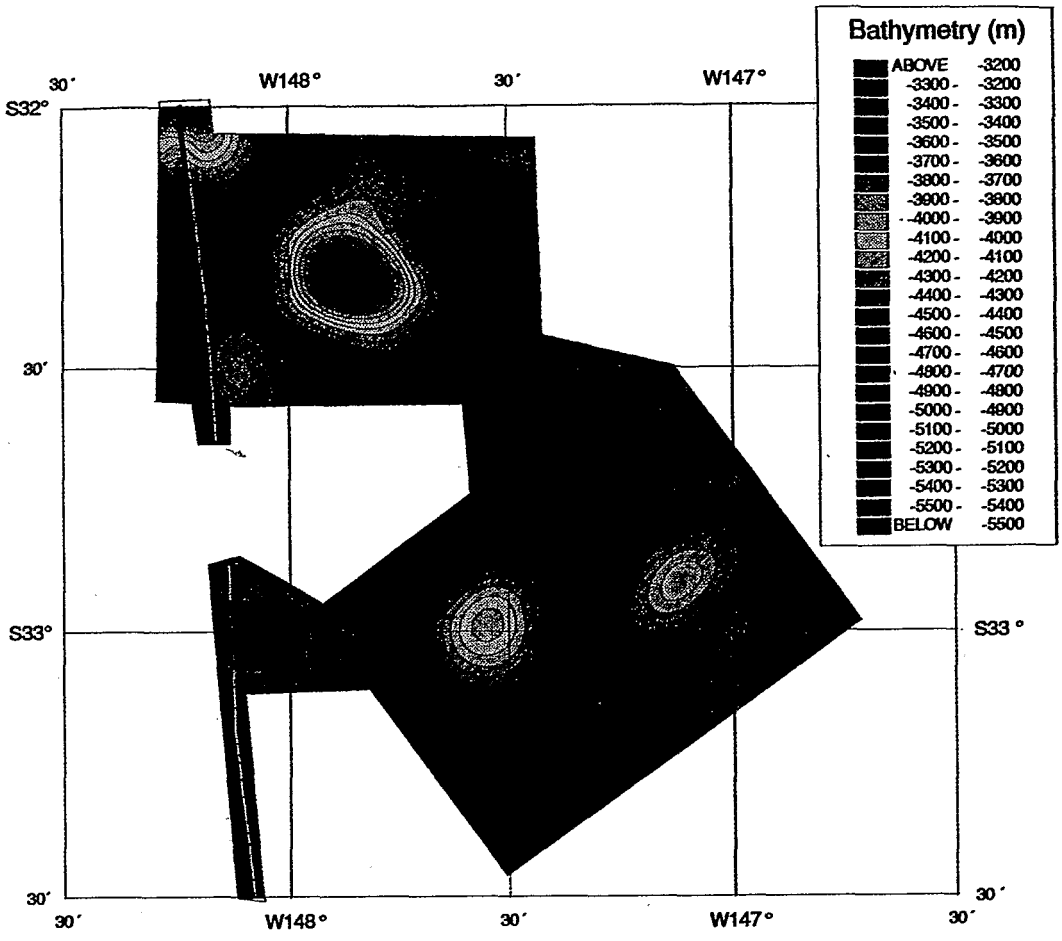

Fig. 10. Bathymetric map obtained by contouring the computed bathymetry on the two computing grids and the Seabeam data. Thick red line is the ship track.

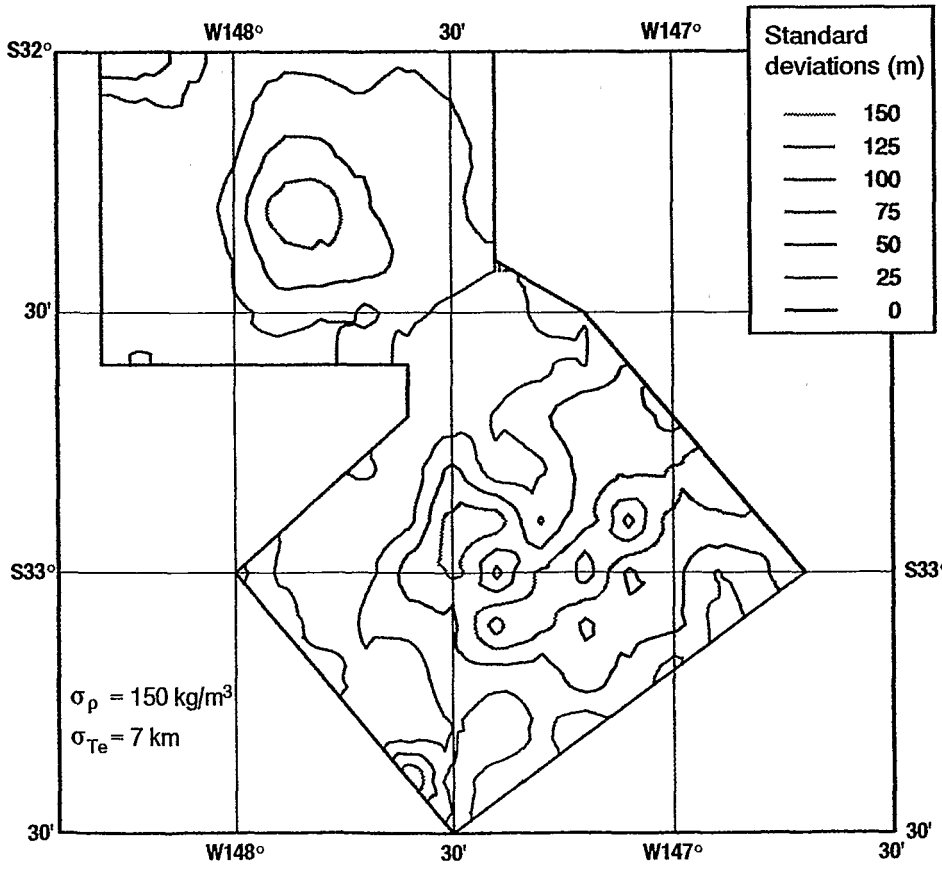

Fig. 11. Standard deviations upon the bathymetry related to the uncertainty on the geophysical parameters used in the computations.

area, the plate deflexion is very small and the uncertainty upon T_e are negligible compared to the deviations due to uncertainty upon the load density. Accordingly, the map of deviations roughly mimics that of the seafloor topography itself by a ratio of about 10%, which is consistent with the ratio between σ_ρ and $(\rho - \rho_0)$.

Conclusions

Before the GEOSAT Geodetic Mission data were declassified in 1992, the spatial distribution of oceanographic satellite tracks was the main factor limiting the performance of detailed bathymetric surveys from satellite altimetry (Baudry and Calmant, 1991). With GEOSAT GM data having been declassified south of latitude 30° S, and with the data from ERS-1 Geodetic Mission, detailed bathymetry surveys can be undertaken in any part of the deep oceans. These surveys can be performed with a 100% coverage in terms of detection and mapping of significant seafloor features. The processing of both satellite altimetry and shipboard echo-sounding bathymetric measurements allows the producing of new bathymetric maps which are a dramatic improvement over the existing global bathymetric maps and digital files. Bathymetric information produced by such processing of both satellite and shipboard data have a wide range of applications in various marine economic activities such as off-shore fisheries, seafloor mineral deposits and petroleum resources assessments.

Acknowledgements

TOPEX/POSEIDON data were obtained from the NASA Physical Oceanography Distributed Active Archive Center at the Jet Propulsion Laboratory/California Institute of Technology and AVISO Operations Center at CLS/CNES France. ERS-1 data were kindly provided by A. Cazenave at GRGS/CNES France. GEOSAT GM data were obtained from NOAA National Oceanographic Data Center. Authors thank J. Bonneau for manuscript preparation.

References

Banks, R. J., Parker, R. L. and Huestis, S. P., 1977, Isostatic Compensation on a Continental Scale: Local Versus Regional Mechanisms, *Geophys. J. Roy. Astr. Soc.* **51**, 431–452.

Baudry, N. and Calmant, S., 1991, 3-D Modelling of Seamount Topography from Satellite Altimetry, *Geophys. Res. Letters* **18**, 1143–1146.

Baudry, N., Diament, M. and Albouy, Y., 1987, Precise Location of Unsurveyed Seamounts in the Austral Archipelago Area Using SEASAT Data, *Geophys. J. Roy. Astr. Soc.* **89**, 869–888.

Calmant, S., 1994, Seamount Topography by Least-Squares Inversion of Altimetric Geoid Heights and Shipborne Profiles of Bathymetry and/or Gravity Anomalies, *Geophys. J. Int.* **119**, 428–452.

Calmant, S., Francheteau J. and Cazenave, A., 1990, Elastic Layer Thickening wih Age of the Oceanic Lithosphere: A Tool for Prediction of the Age of Volcanoes or Oceanic Crust, *Geophys. J. Int.* **100**, 59–67.

Calmant, S. and Baudry, N., 1996, Modelling the Bathymetry by Inverting Satellite Altimetry Data: A Review, *Marine Geophys. Res* **18**, 123–134 (this issue).

Dixon, T. E. and Parke, M. E., 1983, Bathymetry Estimates in the Southern Oceans from SEASAT Altimetry: *Nature* **304**, 406–408.

Jung, W. Y. and Vogt, P. R., 1992, Predicting Bathymetry from GEOSAT-ERM and Shipborne Profiles in the South Atlantic Ocean, *Tectonophysics* **210**, 235–253.

Moritz, H., 1978, Least Squares Collocation, *Reviews of Geophys. and Space Phys.* **16**, 421–430.

Pacific Islands Pilot,1982, Volume III, Islands of the Central Part of the Pacific Ocean: Hydrographer of the Navy.

Oldenburg, D. W., 1974, The Inversion and Interpretation of Gravity Anomalies: *Geophysics* **39**, 526–536.

Parker, R. L., 1972, The Rapid calculation of Potential Anomalies, *Geophys. J. Roy. Astr. Soc.* **31**, 447–455.

Reigber, C., Balmino, G., Muller, H., Bosch, W. and Moinot, B., 1985, GRIM Gravity Model Improvement Using LAGEOS (GRIM3-L1), *J. Geophys. Res.* **90**, 9285–9299.

Sandwell, D. T., 1984, A Detailed View of the South Pacific Geoid from Satellite Altimetry, *J. Geophys. Res.* **89**, 1089–1104.

Sandwell, D. T., 1991, Geophysical Applications of Satellite Altimetry, *Reviews of Geophysics, Suppl., US National Report to International Union of Geodesy and Geophysics 1987–1990*, pp 132–137.

Smith, W. H. F. and Sandwell, D. T., 1994, Bathymetric prediction from Dense Satellite Altimetry and Sparse Shipboard Bathymetry, *J. Geophys. Res.* **99**, 21803–21824.

Vogt, P. R. and Jung, W. Y., 1991, Satellite Radar Altimetry Aids Seafloor Mapping, *EOS Trans. Am. Geophys. Union* **72**, 465,468–469.

Watts, A. B., 1978, An Analysis of Isostasy in the World's Oceans, 1. Hawaiian-Emperor Seamount Chain, *J. Geophys. Res.* **83**, 5989–6004.

Watts, A. B. and Ribe, N., 1984, On Geoid Heights and Flexure of the Lithosphere at Seamounts, *J. Geophys. Res.* **89**, 11,152–11,170.

Marine Geophysical Researches / *Volume 18 Nos. 2–4 June 1996*

Special Issue

Seafloor Mapping in the West, Southwest and South Pacific: Results and Applications

Guest Editors
JEAN-MARIE AUZENDE and JEAN-YVES COLLOT